Histol Histopathol (2016) 31: 51-62

http://www.hh.um.es

Histology and Histopathology

From Cell Biology to Tissue Engineering

Dimensions of compartments and membrane surfaces in the intact rabbit heart of importance in studies on intramyocardial transfer of blood-borne substances

Ger J. van der Vusse[1], Fons Verheyen[2], Robert S. Reneman[1] and Theo Arts[3]

Departments of [1]Physiology, [2]Molecular Cell Biology, ELMI Unit and [3]Biomedical Engineering, Cardiovascular Research Institute Maastricht (CARIM), Maastricht University, Maastricht, the Netherlands

Summary. Cardiac studies on the uptake, storage and intramyocardial transfer of blood-borne substances require detailed information on the geometric ultrastructural dimensions of myocardial compartments and parts thereof, and the membranes separating these compartments. Such a specific ultrastructural set of data of the heart is yet lacking. In the present study, we quantitatively assessed these dimensions in glutaraldehyde-perfusion fixed rabbit hearts by means of histological and tailored mathematical techniques.

We showed the true ellipsoid nature of the myocardial capillary cross section and estimated the mean capillary diameter d_{cap}. After correction for the ellipsoid shape, d_{cap} was found to be 5.21±1.41 μm. Effective widths of the endothelial cell and the pericapillary interstitium (*is*1), dimensions of importance in diffusion, amounted to 187±7 and 160±10 nm, respectively. The fractional volume of the large vessels (arteries and veins larger than 10 μm), capillaries, endothelium, *is*1, cardiomyocytes, non-pericapillary interstitium *is*2, t-tubular compartment and interstitial cells amounted on average to 5.92%, 9.36%, 1.83%, 1.94%, 73.07%, 5.97%, 0.95% and 0.96%, respectively, of total myocardial volume, defined as the cardiac tissue volume, the large blood vessels included. Normalized to total myocardial volume, the surface area of the luminal and abluminal endothelial membranes and of the cardiomyocyte membrane opposing the endothelial cells amounted to $75.2\pm5.5\times10^3$, $82.2\pm6.0\times10^3$ and $89.1\pm6.5\times10^3$ m^2/m^3, respectively.

The present study provides quantitative information about ultrastructural dimensions of the adult rabbit heart, among others, of importance for studies on cardiac uptake, and intramyocardial transfer and storage of blood-supplied substances.

Key words: Rabbit heart, Ultrastructure, Endothelium, Interstitial compartment, Cardiomyocyte

Introduction

Blood-borne substrates and pharmaceuticals generally reach the cardiomyocytes in sufficient quantities to fulfill their function. These substances may differ substantially in hydrophilicity and lipophilicity and, hence, in the mechanisms underlying their transfer from the capillary compartment to cardiac muscle cells. Hydrophilic substrates, like glucose and lactate, bypass

Offprint requests to: Ger J. van der Vusse, Ph.D., Department of Physiology, CARIM, Maastricht University, PO 616, 6200 MD, Maastricht, the Netherlands. e-mail: vandervusse@maastrichtuniversity.nl

DO: 10.14670/HH-11-661

Abbreviations. *LoMagLm*: Low magnification light microscopy; *LoMagEm*: Low magnification electron microscopy; *HiMagEmCf*: High magnification electron microscopy, cross-fiber; *HiMagEmPf*: High magnification electron microscopy, parallel to fiber.

Symbols. *A*: (m^2) Area; *d*: (m) Diameter; *E*: Eccentricity; *h*: (m) Width; *L*: (m) Contour length; *S*: (m^{-1}) Surface area density (m^2/m^3); *s*: (m) Perimeter; *VF*: Volume fraction.

Subscripts. *cap*: Capillary, diameter <10 μm; *ec*: Endothelium, endothelial cell; *ic*: Interstitial cell; *im*: Image area; *is*1: Pericapillary interstitium; *is*2: Non-pericapillary interstitium; *lv*: Large vessel, diameter >10 μm; *myo*: Cardiomyocyte; *diff*: Diffusion related; *tis*: Tissue (=*tot*, excluding *lv*); *tot*: Myocardium including large vessels (*lv*); *ttub*: T-tubuli

the endothelial cells mainly by convective transfer through the endothelial clefts. On the contrary, lipophilic substances, such as fatty acids, have to cross the endothelium by diffusion through the endothelial cell membranes and the endothelial cell interior, since transfer through the clefts is heavily impeded (van der Vusse et al., 2002). The precise nature of the mechanism underlying the uptake of lipophilic substances from the capillary compartment and the subsequent intra-cardiac transfer, however, is still incompletely understood.

Elucidating the mechanisms underlying the uptake, and intramyocardial transfer and storage of lipophilic substances as well as to appreciate to what extent the various barriers might limit their transfer is difficult to accomplish in physiological experiments on the intact heart, considering the complexity of the cellular and subcellular processes involved. A system biology approach, including mathematical modelling, is an alternative to obtain insight into the uptake and transfer of blood-borne substances in the heart. Such an approach requires detailed information about the dimensions of the various compartments, the membrane surface areas and particularly the associated diffusion distances

As illustrated in Fig. 1, a number of distinct compartments and the membranes separating these compartments have to be considered in the uptake and intra-cardiac transfer of blood-borne substances. Capillaries (*cap*) are surrounded by a sequence of structures to be crossed to reach the cardiomyocyte (*myo*) interior, i.e., the endothelium (*ec*), the thin pericapillary interstitium (*is*1), and the cardiomyocyte membrane, i.e., the sarcolemma enclosing the cytoplasm of the cardiac muscle cell. The endothelium comprises the luminal membrane, the endothelial cell interior and the abluminal membrane.

For a given substance, permeability of a barrier

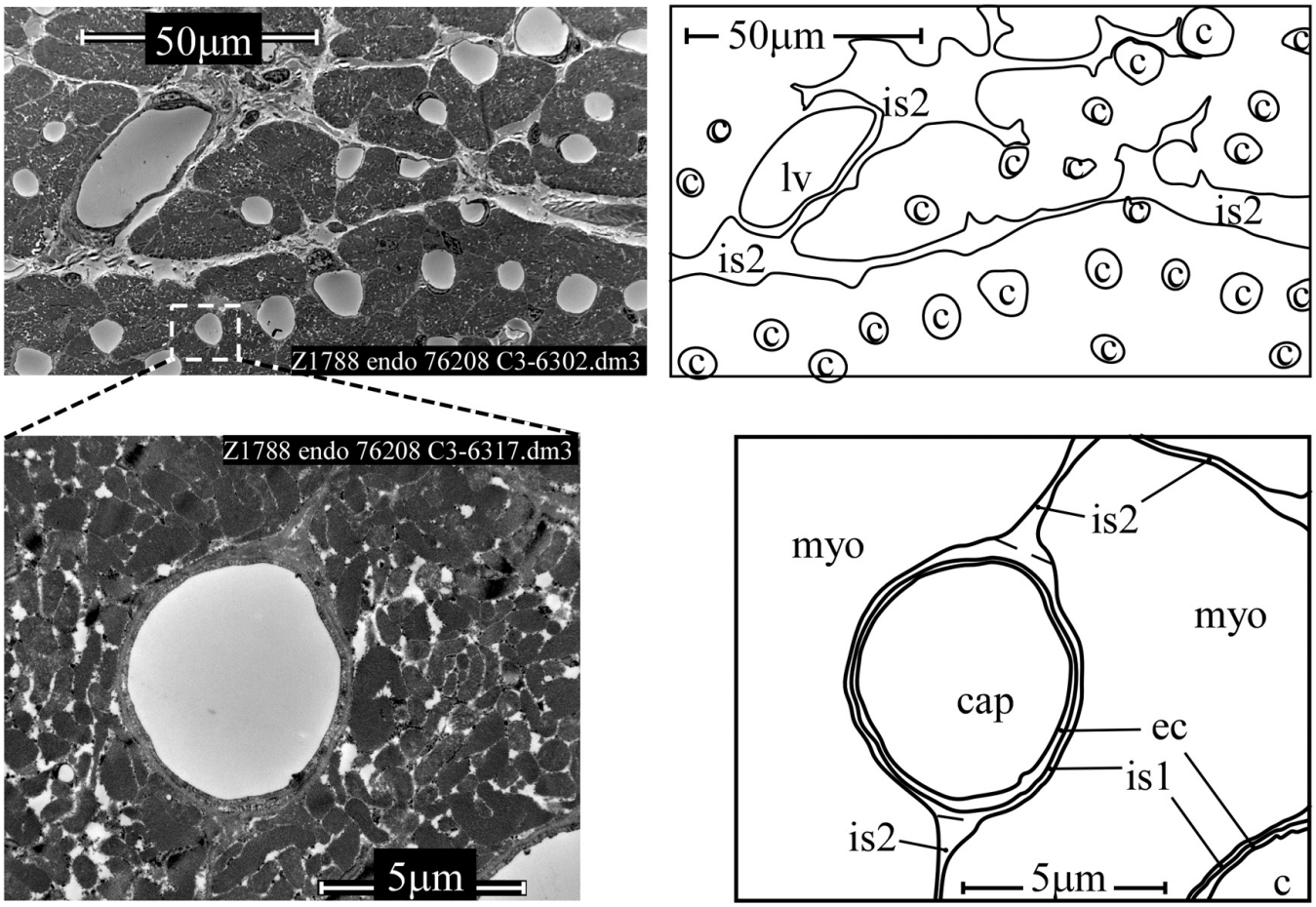

Fig. 1. Typical representation of myocardial ultrastructure. Upper left: low-magnification EM image (*LoMagEm*) of a cross-section of myocardial tissue. Upper right: corresponding schematic drawing of the visible compartments. Capillaries *c*, a large vessel *lv* and visible parts of non-pericapillary interstitium *is2* are indicated. Lower left: high-magnification EM image (*HiMagEmCf*) of a capillary cross-section, corresponding in size to the inset in the upper left panel. Lower right: corresponding schematic drawing of a capillary and its surroundings. Capillaries *cap* are surrounded by endothelium *ec*, pericapillary interstitium *is*1 and cardiomyocytes myo. In between cardiomyocytes, the non-pericapillary interstitium *is2* is located.

depends on the barrier dimensions, i.e., thickness and surface area of the cellular membranes, and the diffusion coefficient for that substance in the barrier material. For full understanding of the mechanisms underlying cardiac uptake and intra-myocardial transfer of substances, the storage capacity of the various compartments in the heart has to be known as well. The storage capacity of these compartments depends on their anatomical volume and the binding characteristics of the substances to the proteins present in these compartments, if any.

Unfortunately, such a detailed set of specific ultrastructural geometrical data is not provided in previous studies on the quantification of ultrastructural dimensions of the heart (Frank and Langer, 1974; Vinnakota and Bassingthwaighte, 2004). Moreover, previously presented data appeared to be controversial, especially regarding the volumes of the capillaries and the interstitial compartments, parameters highly relevant for uptake, transfer and/or storage of blood-supplied substances. Besides, in these studies (McElroy et al., 1978; O'Keefe et al., 1978; Anversa et al., 1983; Gonzalez and Bassingthwaighte, 1990; Judd and Levy, 1991), no distinction was made between the pericapillary interstitium, *is*1, and the non-pericapillary interstitium, *is*2. Distinction between these compartments is essential, because the former is the site of preference for the exchange of blood-borne lipophillic substrates between capillaries and cardiomyocytes, while the latter mainly serves as the storage site.

The main objective of our study is to quantify the ultrastructural geometric dimensions of the compartments and membranes separating these compartments within the left ventricle of the rabbit heart, playing an important role in the uptake, storage and intramyocardial transfer of blood-supplied substances. We derived these ultrastructural geometric data from light and electron microscopic images of isolated, glutaraldehyde-perfusion fixed adult rabbit hearts. We obtained quantitative information from these microscopic data by application of tailored mathematical techniques, largely based on statistical averaging of segment lengths and surface areas measured in randomly selected microscopic images.

Materials and methods

Animals and heart perfusion

Experiments were performed with approval of the Animal Ethical Committee of Maastricht University (#2010-094) in accordance with the Guide for the Care and Use of Laboratory Animals published by the US National Institutes of Health (NIH Publication No. 85-23 revised 1996). Three female adult white New Zealand rabbits were included in the study. The animals, aged around 3 months, were anaesthetized with an intramuscular (i.m.) injection of 1.5 ml ketamine solution (100 mg/ml; Eurovet, Bladel, the Netherlands). After 10 min 1 ml medetomidine hydrochloride solution was injected i.m. (1 mg/ml; Eurovet), 10 min later followed by injection of 1 ml heparin into the marginal ear vein (5000 U/ml; Leo Pharma, Balarup, Denmark). Subsequently, the animals were sacrificed by cervical dislocation. After opening of the thorax, the heart was extirpated and mounted on a Langendorff-perfusion apparatus via the aortic stump. The heart was immediately perfused with a modified Krebs-Ringer-Henseleit buffer (120 mM NaCl, 2.5 mM KCl, 1.5 mM KH_2PO_4, 1.2 mM $MgSO_4.7H_2O$, 10 mM HEPES, 9.5 mM glucose and 1 mM $CaCl_2$; pH 7.4 and oxygenated with 100% O_2) at 37ºC for 5 min to remove blood from the coronary vessels. Perfusion pressure amounted to 75 mmHg; flow rate of the buffer solution was approximately 40 ml/min.

Tissue preparation for Light and Electron microscopy

Five min after the start of rinsing out blood, the hearts were perfused with 3% glutaraldehyde buffered with 90 mM KH_2PO_4, pH 7.4, at room temperature. Flow rate was approximately 10 ml/min. After 5 min perfusion, the glutaraldehyde-fixed heart was removed from the perfusion apparatus and the left ventricle was divided into five equally thick slices from base to apex. Subsequently small samples (approximately 3x3x1 mm) were randomly taken from these slices at various locations throughout the left ventricular wall. The samples were further fixed in the phosphate-buffered glutaraldehyde solution for at least one week. After an overnight rinse in 90 mM KH_2PO_4 buffer supplemented with 7.5% sucrose, the samples were post-fixed in 2% OsO_4 in 0.1 M veronal-acetate buffer (pH 7.4) supplemented with 1.5% ferricyanide at 4°C for 1 h. After a short rinse in a veronal-acetate buffer containing 7% sucrose, the samples were dehydrated through a graded series of ethanol and routinely processed before embedding in Epon resin. Subsequently, semi-thin sections (1 μm thick) were stained with Periodic acid-Schiff (PAS) and toluidine blue for light-microscopic (LM) evaluation. Ultra-thin sections of about 60 to 75 nm thick were stained with uranyl acetate and lead citrate before examination in a Philips CM100 electron microscope (EM).

Images of tissue sections

Series of images were obtained from the left ventricular myocardium. Volume fractions were quantified by measuring surface areas in randomly selected images, normalized to the surface area of total myocardium, for the following compartments: capillaries (*cap*), endothelium (*ec*), pericapillary interstitium (*is*1), non-pericapillary interstitium, i.e., interstitium in between cardiomyocytes (*is*2), cardiomyocytes (*myo*), large blood vessels (arteries and veins larger than 10 μm) (*lv*) and interstitial cells (*ic*). Taking into account that myocardial tissue is highly anisotropic, capillaries, endothelium and pericapillary interstitium were

considered to be concentric tubular structures with a slightly elliptic cross-section. In images of slices perpendicular to the fiber direction we measured the length of membrane cross-sections, permitting the estimation of the surface area densities (normalized to total myocardial tissue) of cell membranes, i.e., the luminal and abluminal endothelial membrane and the sarcolemma. Furthermore, in these images the widths of *ec*, *is*1 and *is*2 were determined. In this way, we obtained 3-dimensional quantitative information from 2-dimensional pictures, following as closely as possible the most recent principles of stereology (Mandarim-de-

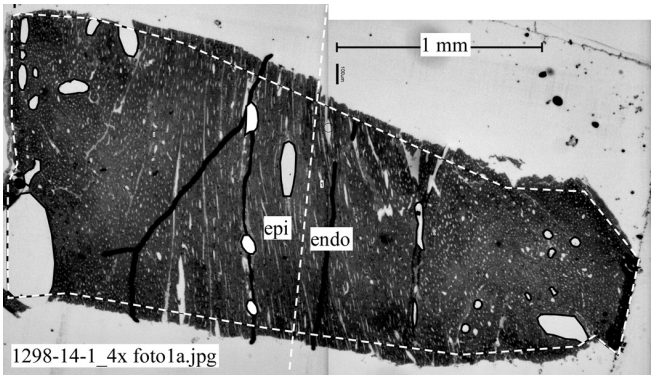

Fig. 2. Low magnification light microscopic photograph (*LoMagLm*) of a transmural section of rabbit left ventricular myocardium. The figure is composed of two images. The subepicardial (*epi*) and subendocardial (*endo*) regions are shown on the left and right hand side, respectively. We considered lumen diameters exceeding 10 *μ*m to belong to non-capillary, large vessels. We outlined these vessels in black and calculated their area fraction relative to total area, outlined by the white dashed lines.

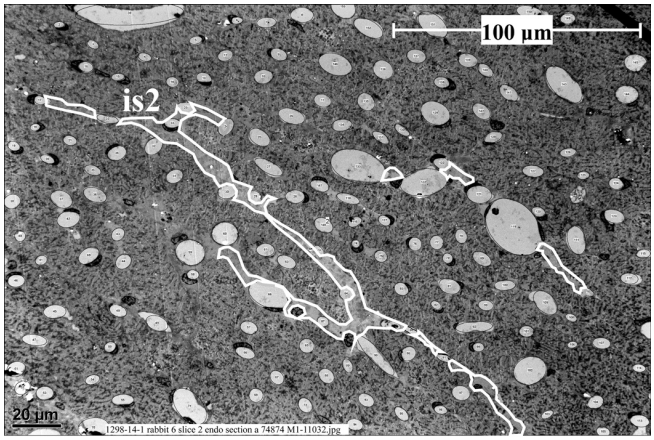

Fig. 3. Low magnification electron microscopic photograph (*LoMagEm*) of rabbit left ventricular myocardium. Tissue is cut perpendicularly to the fiber orientation. Non-pericapillary interstitium, *is*2, is outlined in white. In all capillary cross-sections, the best-fit ellipses are drawn in black. Large blood vessels or fractions thereof, *lv*, are contoured as well.

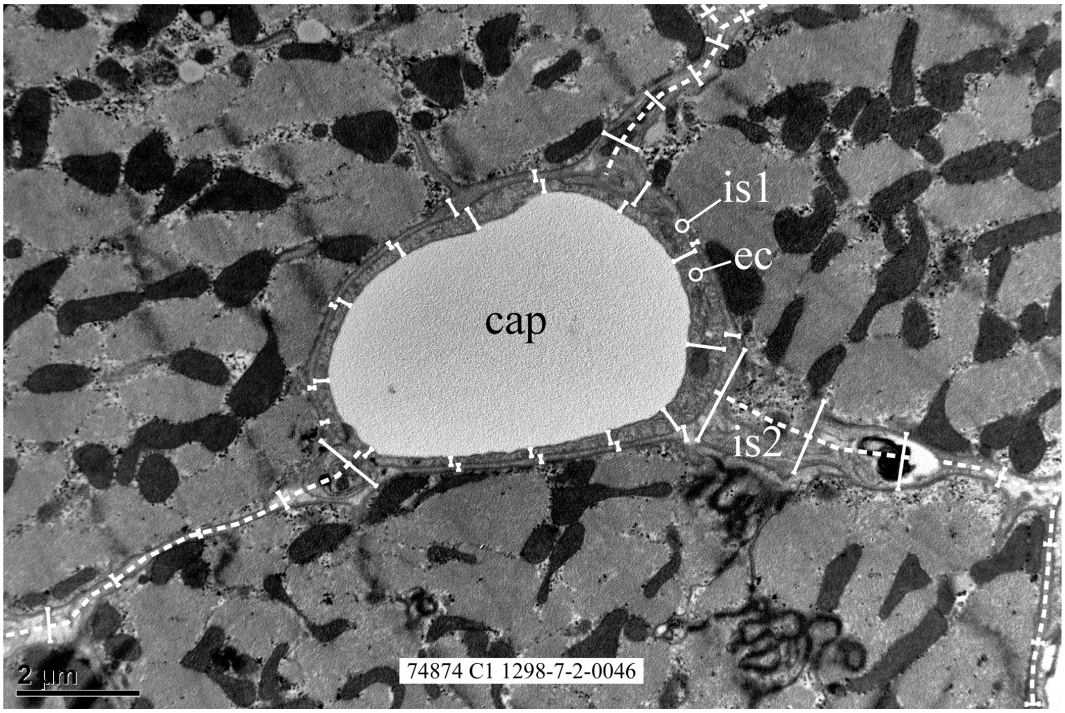

Fig. 4. High magnification electron microscopic image (*HiMagEmCf*) of rabbit left ventricular myocardium. Tissue is cut perpendicularly to the fiber orientation. Around the capillaries (*cap*), a layer of endothelial cells (*ec*) and the interstitium between endo-thelium and cardio-myocytes (*is1*) is visible. At distances of about 1 μm along the capillary perimeter, samples were taken for *ec* and *is*1 width determinations, as indicated by short white bars. We also measured the lengths of the capillary perimeter and of the center-line (dashed line) of the non-pericapillary interstitium *is*2, as far as visible on the image under study. The width of the *is*2 layer was measured along the short white bars drawn perpendicularly to the centre line with a sample distance of approximately 1 μm.

Lacerda, 2003; Muhlfeld et al., 2010). We analyzed the images with the software package ImageJ 1.45s (NIH, http://rsb.info.nih.gov/ij). Areas were determined by using an electronic grid counting the number of pixels.

Low magnification light microscopic images *LoMagLm* of cross-fiber sections (3840x3075 pixels, 1 mm=1800 pixels, Fig. 2) were used to evaluate tissue quality and to estimate the volume fraction of large vessels (*lv*). In each section, areas of large vessels, the short axis of which in cross-sections exceeded 10 µm, were added up to obtain total large vessel area from which large vessel volume was derived as indicated below in Equation 2.

In low magnification electron microscopic images of cross-fiber sections *LoMagEm* (3840x3075 pixels, 100 µm=2920 pixels, Fig. 3) we determined the best-fit ellipses of all capillary cross-sections. By visual inspection for each capillary the major and minor axes and the angulation of the ellipse template were adjusted until the best-fit ellipse was obtained, making use of the ImageJ software package. In addition, we marked the non-pericapillary interstitium (*is*2), visible on these images, by contouring. We also contoured the visible fraction of *lv*, if any, on these images. We obtained the fractional area of both the capillary lumen, A_{cap}, and the non-pericapillary interstitium, *is*2, by normalizing their respective areas to total area minus the area of *lv*. The fraction of *is*2 assessed on *LoMagEm* images was added to that of *is*2 assessed at higher magnification (*HiMagEmCf*; see below) for calculation of the total volume fraction of *is*2, using Equation 11.

In high magnification electron microscopic images *HiMagEmCf* of cross-fiber sections (3798x2532 pixels, 10 µm=2200 pixels, Fig. 4) we determined the widths of the endothelium (*ec*), the pericapillary interstitium (*is*1) and the non-pericapillary interstitium (*is*2). For these measurements, the sampling distance along the centerline was approximately 1 µm. We also determined the ratio of the length of the non-pericapillary interstitial centerline and the length of the capillary perimeter (L_{is2}/L_{cap}), as far as visible, on the image under investigation. Furthermore, in these images, the area fraction of interstitial cells *ic* was determined.

In high magnification electron microscopic images of parallel (*HiMagEmPf*) fiber sections (3798x2532 pixels, 10 µm= 2200 pixels, Fig. 5) we determined the ratio of total T-tubuli (*ttub*) cross-sectional area and cardiomyocyte area (A_{ttub}/A_{myo}).

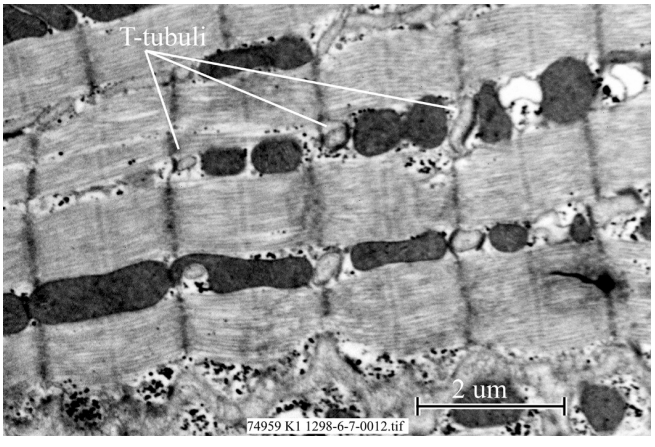

Fig. 5. Enlarged detail of a high magnification electron microscopic image (*HiMagEmPf*) of rabbit left ventricular myocardium. Tissue is cut parallel to the fiber orientation. The periodic pattern of the sarcomeres with dark Z-lines is clearly visible. Cross-sections of a number of T-tubuli are indicated. These structures are generally present between the myofilaments near the Z-lines.

Calculation of capillary diameter, widths of aqueous layers, membrane surface areas and volume fractions of intra-/extracellular compartments

Capillary diameter and volume

As mentioned above in relation to Fig. 3, in the *LoMagEm* images, we determined the best fitting ellipses for all capillary contours in the image, providing the length of the long (d_{max}) and short (d_{min}) axes and the angulation (α) of the long axis relative to the horizontal of the image. The ellipticity of the capillary cross-section is the summed effect of oblique cross-sectioning and real ellipticity of the capillary cross-section. Capillary diameter d_{cap} (equation 1) and ellipticity *E* were defined by:

$$d_{cap} = \sqrt{d_{\max}\ d_{\min}} \qquad E = \ln(d_{\max} / d_{\min})$$

Capillary diameter was defined so that the area of a circle with diameter d_{cap} equals the area of the true ellipsoidal cross-section of the capillary. In the *LoMagLm* images, we contoured the tissue, including the large vessels, rendering total tissue area A_{tot}. We also contoured the large vessels separately, rendering large vessel area $A_{lv,Lm}$. Using the stereological principle that the ratio of cross-sectional areas *A* equals the ratio of volume fractions *VF* (equation 2), we applied:

$$VF_{lv} = A_{lv,Lm} / A_{tot}$$

In the *LoMagEm* images, we determined tissue area A_{tis} without large vessel and the ellipsoidal contours of all capillaries. For each capillary, cross-sectional area $A_{cap,i}$ was determined, where *i* refers to capillary numbering. From these images, we obtained the ratio of volume fractions of the capillaries VF_{cap} relative to that of the tissue (*tis*) without large vessels (*lv*). Using VF_{lv}, as determined on *LoMagLm* images by Equation (2), for VF_{cap} (equation 3) it holds that:

$$VF_{cap} = \frac{(1 - VF_{lv})}{A_{tis}} \sum_i A_{cap,i}$$

Widths of aqueous compartments

Substances like fatty acids, moving from capillary lumen to cardiomyocyte, cross the *ec* and *is*1 compartments by facilitated diffusion (Bassingthwaighte et al., 1989). Thin aqueous layers represent these two compartments, i.e., the cytoplasm of the endothelium and that of the pericapillary interstitium between endothelium and cardiomyocyte. We measured the width of these compartments at regular distances around the capillary perimeter in *HiMagEmCf* images, as indicated in detail in the Legend to Fig. 4. It should be emphasized, that for describing diffusion through these layers the average width h is not relevant, but the diffusion-related width h_{diff}, i.e., the inverse of the average inverse width, analogous to the calculation of parallel electrical resistance. Diffusion-related widths $h_{diff,ec}$ and $h_{diff,is1}$, associated with the *ec* and *is*1 compartments, respectively, were calculated accordingly. We estimated the average width h_{is2} of the non-pericapillary interstitium *is*2 from the data obtained in *HiMagEmCf* images. To this end, a centerline in the *is*2 compartment was drawn and the width of the compartment was measured at regular intervals of about 1 μm along the centerline, as indicated in the Legends of Fig. 4.

Membrane surface areas

For estimation of permeability associated with diffusion of substances from capillary lumen to the cardiomyocyte interior, the surface area of the boundaries between the compartments has to be known. Surface area density, defined as the surface area per total tissue volume, was estimated for the three pericapillary membranes between the compartments *cap* and *ec*, *ec* and *is*1 and *is*1 and *myo*. Corresponding symbols are $S_{cap,ec}$, $S_{ec,is1}$, and $S_{is1,myo}$, respectively. We assumed that the ratio $S_{cap,ec}/VF_{cap}$ equals the ratio of capillary perimeter and cross-sectional area of the capillary lumen. Knowing the mean capillary diameter d_{cap} and the mean eccentricity E_{cap} of the capillary cross-section, the circumference of the ellipsoidal capillary cross-section was found to be slightly larger than the circumference of a circle with diameter d_{cap}. As derived in the Appendix, the related correction factor equals the square root of cosh (E_{cap}). So, $S_{cap,ec}$ (equation 4) can be described as a function of VF_{cap}, mean capillary diameter d_{cap} and eccentricity E_{cap} by:

$$S_{cap,ec} = \frac{4VF_{cap}}{d_{cap}} \sqrt{\cosh(E_{cap})}$$

Taking into account that the surface area of the two outer cellular membranes has a larger perimeter than the luminal endothelial membrane due to added thickness h_{ec} and h_{is1} of the compartments *ec* and *is*1, respectively, it follows (equations 5, 6):

$$S_{ec,is1} = S_{cap,ec} \frac{d_{cap} + 2h_{ec}}{d_{cap}}$$

$$S_{is1,myo} = S_{cap,ec} \frac{d_{cap} + 2h_{ec} + 2h_{is1}}{d_{cap}}$$

In addition, we quantified the surface area density of the interstitial layer between the cardiomyocytes, the so-called non-pericapillary interstitium, belonging to compartment *is*2 (S_{is2}). We considered the ratio of the length of the *is*2 centerline and capillary perimeter (L_{is2}/L_{cap}), as determined in the *HiMagEmCf* images (Fig. 4), to represent the surface area ratio of the non-pericapillary interstitial compartment and the capillary wall. Thus, we applied (equation 7):

$$S_{is2} = \frac{L_{is2}}{L_{cap}} S_{cap,ec}$$

Note that to obtain surface area density of the total cardiomyocyte membrane, S_{is2} should be multiplied by 2 and added to the pericapillary surface area density, S_{is1}.

Volume fractions

From the primary measurements, obtained from the images, we estimated volume fractions *VF* of the relevant compartments as indicated below. The sum of all *VFs* equals 1.0, i.e., representing total volume (equation 8):

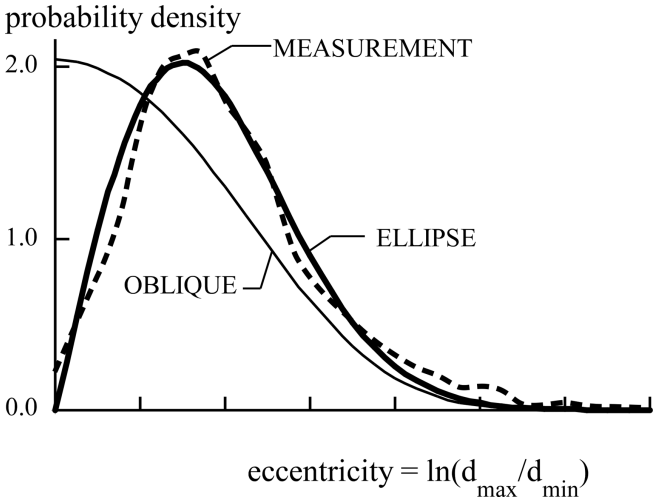

Fig. 6. Probability density functions of the eccentricity of capillary cross-sections. The broken line represents the measured function based on 2338 capillary sections. Model *ELLIPSE* assumes normal distributions of the two eccentricity parameters E_{xx} and E_{xy} of the capillary cross-section (Equation 15). Model *OBLIQUE* attributes eccentricity to oblique sectioning of circular cylindrical capillaries. Because of its discrepancy with experimental findings, we rejected the *OBLIQUE* model.

$$VF_{lv} + VF_{cap} + VF_{ec} + VF_{is1} + VF_{myo} + VF_{is2} + VF_{ttub} + VF_{ic} = 1$$

Volume fractions VF_{lv} and VF_{cap} were determined with Equations (2-3). We determined volume fraction VF_{ec} and VF_{is1} (equations 9, 10) by multiplication of the respective widths and surface area densities, obtained by Equations (4-6):

$$VF_{ec} = \frac{1}{2} h_{ec} (S_{cap,ec} + S_{ec,is1})$$

$$VF_{is1} = \frac{1}{2} h_{is1} (S_{ec,is1} + S_{is1,myo})$$

As indicated above, the *is*2 compartment represents the interstitial layer between the cardiomyocytes. At some locations, *is*2 is so wide that we were able to contour this compartment on the low magnification images *LoMagEm* (Fig. 3). In these images, however, most other parts of the *is*2 layer, separating individual cardiomyocytes, were too thin to be visible at this magnification. Therefore, we measured the width h_{is2} of the non-pericapillary interstitial layer *is*2 also on the high magnification *HiMagEmCf* images at multiple points and at regular sampling distances (see Legends to Fig. 4). The surface area of this layer was determined with Equation (7). Since most h_{is2} measurements were obtained at locations where this layer is relatively thin, we decided to use the median rather than the mean value of h_{is2} for calculating this part of the *is*2 volume. We found total *is*2-volume by adding up the latter volume to the *is*2 volume determined on the *LoMagEm* image, calculated with a method similar to that used in the assessment of VF_{cap} (Equation 3). Thus, it follows that (equation 11):

$$VF_{is2} = S_{is2} median(h_{is2}) + \frac{(1 - VF_{lv}) A_{is2}}{A_{tis}}$$

In the *HiMagEmCf* images, we determined the area A_{im} of the image and A_{ic} of the interstitial cells. The image was considered to represent tissue without large vessels; hence, the volume fraction of the interstitial cells is (equation 12):

$$VF_{ic} = \frac{(1 - VF_{lv}) A_{ic}}{A_{im}}$$

In *HiMagEmPf* images (Fig. 5), we assessed the area of the cardiomyocyte A_{myo} and the total area of all T-tubules A_{ttub}. We calculated the related volume fractions by (equation 13):

$$VF_{myo} = \frac{VF_1 A_{myo}}{A_{myo} + A_{ttub}} \qquad VF_{ttub} = \frac{VF_1 A_{ttub}}{A_{myo} + A_{ttub}}$$

with:

$$VF_1 = 1 - (VF_{lv} + VF_{cap} + VF_{ec} + VF_{is1} + VF_{is2} + VF_{ic})$$

Volume fraction VF_1 represents all volume fractions without those of the compartments *myo* and *ttub*.

Results

Primary measurements

Table 1 summarizes the primary measurements as obtained from the hearts under investigation. The table shows mean values and standard deviations (unless otherwise indicated) and the number of images analyzed within parentheses. Because no differences between subendo- and subepicardial layers could be detected, data are presented for the complete left ventricular wall.

Table 1. Primary measurements in the rabbit left ventricular myocardial wall.

LoMagLm	A_{lv}/A_{tot} [-]	0.059±0.021 (27)
LoMagEm	A_{cap}/A_{tis} [-]	0.094±0.029 (21)
	A_{is2}/A_{tis} [-]	0.041±0.030 (21)
	d_{cap} [µm]	5.21±1.41 (2338)
	$d_{min,cap}$ [µm]	4.63±1.13 (2338)
HiMagEmCf	h_{ec} [nm]	244±192 (34)
	$h_{ec,diff}$ [nm]	187±140 (34)
	h_{is1} [nm]	237±221 (34)
	$h_{is1,diff}$ [nm]	160±147 (34)
	h_{is2} [nm]	339±358 (34)
	h_{is2} (median) [nm]	203
	L_{is2}/L_{cap} [-]	1.25±0.56 (87)
	A_{ic}/A_{tis} [-]	0.010±0.022 (40)
HiMagEmPf	A_{ttub}/A_{myo} [-]	0.013±0.004 (16)

LoMagLm, low magnification light microscopy; *LoMagEm*, low magnification electron microscopy; *HiMagEmCf* and *HiMagEmPf*, high magnification electron microscopy cross- and parallel fiber, respectively; data, mean±sd; n, number of images studied, except for d_{cap} (n, number of capillaries measured); (-), unit less. *A*, area; *d*, diameter; *h*, width; h_{diff}, diffusion-related width; *L*, contour length. Subscripts: *cap, ec, is1, is2, ttub, lv, ic, tis, tot*: see list of symbols. Note that we calculated the median of h_{is2} for use in Equation (11).

Table 2. Volume fractions, surface areas and layer widths in the rabbit left ventricular myocardium.

Compartment	Abbreviation	Volume fraction VF [%]	Width *h* [nm]	Diffusion width h_{diff} [nm]
Capillaries	*cap*	9.36±0.67		
Endothelium	*ec*	1.83±0.15	244±10	187± 7
Pericapillary interstitium	*is1*	1.94±0.15	237±12	160±10
Non-pericapillary interstitium	*is2*	5.97±0.69	339±15	
Cardiomyocytes	*myo*	73.07±1.45		
T-tubules	*ttub*	0.95±0.08		
Large blood vessels	*bv*	5.92±0.84		
Interstitial cells	*ic*	0.96±0.32		

See for abbreviations for the compartments: "List of symbols and abbreviations"; data, mean ± SEM.

In Table 2, we summarize the volume fractions and widths of the aqueous compartments, as calculated from the primary data. Volume fraction of the capillary lumen (FV_{cap}) was on average 9.36%. On average, the volume fraction of large vessels amounted to 5.92%. Hence, total vessel volume, being the sum of the volumes of the capillary (FV_{cap}) and large vessel (FV_{lv}) compartments, was on average about 15.5% of the total volume. It should be noted that we considered all vessels with a diameter smaller than 10 μm as capillaries and with a diameter larger than 10 μm as large vessels. The range of the latter ones was 10 till 400 μm. The volume fraction of the capillary interstitial compartment, FV_{is1}, *is*1 being the compartment between endothelium and cardiomyocytes, was on average 1.94%. The volume fraction of the non-pericapillary interstitial compartment, FV_{is2}, *is*2 being the interstitial compartment between cardiomyocytes, and of the T-tubular compartment, FV_{ttub}, *ttub* being the interstitial compartment within cardiomyocytes, was on average 5.97% and 0.95%, respectively. The total interstitial fractional volume, i.e., the sum of *is*1, *is*2 and *ttub*, was about 8.9%. The fractional volume of the endothelial cells (FV_{ec}), the interstitial cells (FV_{ic}) and the cardiomyocytes (FV_{myo}) was on average 1.83%, 0.96 and 73.1%, respectively. The average widths of the compartments ec and *is*1 were of the same order of magnitude (on average 244 and 237 nm, respectively). The diffusion-related widths of ec and *is*1, also shown in table 2, were always smaller than the corresponding average widths. On average, they amounted to 187 and 160 nm, respectively.

The surface area density, i.e., the surface area of the capillary wall normalized to total volume, of the luminal endothelial membrane (*cap-ec*) was on average 75.2x10^3 m^2/m^3 (Table 3). The surface area densities of the abluminal endothelial membrane (*ec-is*1) and the cardiomyocyte membrane opposing the endothelial cells (*is*1-*myo*) were somewhat larger than that of the luminal endothelial membrane, on average 82.2 and 89.1x10^3 m^2/m^3, respectively, because they encapsulate the capillaries (Table 3). The mid-compartment surface area of *is*2 amounted to 94.0x10^3 m^2/m^3. Hence, the total surface area density of the cardiac muscle cell membrane, calculated as $S_{is1,myo}+2S_{is2,myo}$, is 277x10^3 m^2/m^3, ignoring the surface area of the t-tubular system.

Table 3. Intramyocardial surface areas densities.

Surface	Abbreviation	Surface area density [10^3 m^2/m^3]
cap-ec membrane	$S_{cap,ec}$	75.2±5.5
*ec-is*1 membrane	$S_{ec,is1}$	82.2±6.0
*is*1-*myo* membrane	$S_{is1,myo}$	89.1±6.5
*is*2 *mid*-compartment	S_{is2}	94.0±8.7

See for abbreviations for the compartments: "List of symbols and abbreviations". Data, mean ± SEM. Note that i) the *is*2 compartment is bordered by cell membranes of cardiomyocytes on both sides and ii) the *is*2 mid-compartment surface pertains to the surface of an imaginary plane parallel to the enclosing cardiomyocyte membranes

Discussion

In the present study, we investigated quantitatively the dimensions of the compartments and the cellular membranes, separating these compartments, within the left ventricle of the rabbit heart. In particular, we estimated the fractional volumes of endothelial cells, cardiomyocytes, large vessels (arteries and veins), capillaries and interstitial compartments. We also assessed the surface areas of the luminal and abluminal endothelial membranes and the sarcolemma. We chose the rabbit as species of investigation, because functional cardiac studies are increasingly carried out in this species (Saburkina et al., 2014; Waits et al., 2014; Wang et al., 2014) due to the similarities in physiological function of human and rabbit hearts (Blaauw et al., 2010). Needless to say that one has to be careful in extrapolating the present findings as obtained in the rabbit heart to other species.

Normalized to total myocardial wall volume, the capillary fractional volume in the myocardial left ventricle was found to be 9.4%±0.7%. This value is slightly higher than for instance published for rat cardiac tissue by Anversa and colleagues (Anversa et al., 1983) and Judd and Levy (1991), but considerably lower than observed by McElroy and colleagues (McElroy et al., 1978) and O'Keefe and coworkers (O'Keefe et al., 1978) in rat and dog left ventricular tissue (23.6% and 27.2%, respectively). An explanation for the deviant findings in the latter two studies should most likely be sought in the techniques used to visualize the capillary lumen separately from the endothelial cell interior and *is*1 (O'Keefe et al., 1978) or the use of black ink as indicator of the capillary compartment (McElroy et al., 1978).

The fractional volume of the endothelial cells of 1.83%±0.15% as found in the present study on rabbits does not corroborate with previously published data for dog and rat myocardial tissue. In these species, the endothelial fractional volume varied from 2.7 to 4.2% (Gerdes and Kasten, 1980; Anversa et al., 1983). Although an explanation for these deviating data is not at hand, species differences may have to be considered. It is noteworthy that the average anatomical and diffusional widths of the endothelium in the rabbit left ventricular tissue were different; 244±10 nm and 187±7 nm, respectively. We like to emphasize that the value of the diffusional rather than the anatomical width should be considered, when analyzing diffusion of substances through the cardiac endothelial cells.

Little is known about the surface area of the luminal and abluminal endothelial membranes, despite the importance of these membranes for trans-endothelial trafficking of blood-borne and externally applied substances from the capillary lumen via the endothelium to the interstitial compartment. Anversa and coworkers (Anversa et al., 1983) estimated the capillary lumen surface area, normalized to cardiomyocyte volume, in

the rat left ventricle to be about $86x10^3$ m^2/m^3. This value roughly corresponds with $60x10^3$ m^2/m^3, normalized to total volume of the myocardium. In the present study on rabbit left ventricular tissue, however, we found the surface area of the luminal and abluminal endothelial membranes normalized to total volume amounted to $75.2\pm5.5x10^3$ and $82.2\pm6.0x10^3$ m^2/m^3, respectively. These values are notably higher than those found in rat heart (Anversa et al., 1983).

In analyzing the fractional volume of the interstitial compartment in the rabbit left ventricle, we distinguished the interstitium between endothelial cells and the opposing cardiomyocytes (*is*1) from the interstitium in between the cardiomyocytes, the so-called non-pericapillary interstitium (*is*2). The major reason for this distinction is the notion that especially lipophilic compounds, diffusing from the endothelial abluminal membrane towards the cardiomyocytes, will mainly cross *is*1. The non-pericapillary interstitium, *is*2, most likely plays a minor role in trafficking of lipophilic substances from endothelium to cardiomyocyte. To the best of our knowledge, this essential distinction has not been made before. The fractional volume of *is*1 was found to be 1.94%±0.15%, normalized to total myocardial volume. The fractional volume of *is*2 and the t-tubular compartment amounted to 5.97%±0.69% and 0.95%±0.08%, respectively. Therefore, the fractional volume of the total interstitial compartment, i.e., the sum of *is*1, *is*2 and the t-tubular compartment, is approximately 8.9%. It is of note that previous attempts to measure the total interstitial compartment in the myocardium resulted in mutually deviating values. Volumes assessed by means of chemical techniques, i.e., perfusion with markers like inulin, sucrose, Co-EDTA, etc., generally resulted in substantially larger values for the fractional cardiac interstitial volume, varying from 18.8% in rat (Cieslar et al., 1998) to 21.0% in rabbit hearts (Gonzalez and Bassingthwaighte, 1990). However, the present data based on histological measurements in the rabbit heart are in line with previous findings in a variety of species obtained with comparable histological techniques. Fractional volumes of the total interstitial compartment assessed with histological techniques on both *in vivo* and *ex vivo* glutaraldehyde-perfusion fixed rat, rabbit and dog myocardium were found to be approximately 4 to 8% of total myocardium (Frank and Langer, 1974; Gerdes and Kasten, 1980; Anversa et al., 1983). Shrinkage of the interstitial compartment due to glutaraldehyde fixation may cause the difference in outcome between histologically and chemically determined sizes of the interstitium. Data published by Frank and Langer (1974), however, indicate that shrinkage of myocardial tissue caused by the fixation procedure does not exceed 10%. They also suggest that predominantly the cardiomyocytes are subject to fixation-induced shrinkage, a notion substantiated by Eisenberg and Mobley (1975). They showed that shrinkage of isolated muscle fibers subjected to a comparable fixation procedure was about 7 to 28%. These findings obviously indicate that shrinkage of the interstitial compartment due to fixation does not explain the differences between the relatively large and the relatively small size of the interstitial compartment as determined chemically and histologically, respectively. The size of the interstitial compartment can be easily overestimated if the water-soluble chemical markers used are not freely distributed in the aqueous space of the interstitium, but adhere, for example, partly to the glycocalyx of the endothelial cells and/or to the extracellular matrix present in the interstitial compartment. Alternatively, the chemical may gain access to areas within the tissue that morphologically do not belong to the interstitial compartment, as suggested by Macchia and colleagues (1979), Page and Page (1968) and Frank and Langer (1974).

It should be emphasized that swelling of cardiac structures during perfusion with a crystalloid buffer cannot be excluded, hampering the extrapolation of data obtained in crystalloid-buffer perfused hearts to blood-perfused organs. In the present experimental setup, we perfused the rabbit heart with a crystalloid-buffer for about 5 minutes prior to glutaraldehyde fixation. Polimeni and Buraczewski (1988) showed that the size of both the extracellular and intra-cardiomyocyte compartments of the isolated rat heart increases by approximately 30% during crystalloid buffer perfusion for 10 minutes. Based on these findings, the conclusion can be drawn that expressing interstitial volume as a percentage of total myocardial volume, as in the present study, will not affect the quantitative estimation of the size of the interstitial compartment.

It is of note that the average value of the anatomical and diffusional width of *is*1 is different, i.e., 237±12 nm and 160±10 nm, respectively. The latter value must be considered in evaluating the diffusion distance of substances crossing the compartment between endothelium and cardiomyocyte. The diffusional width is substantially smaller than the anatomical width as assessed in the present study and as found by Frank and Langer in the rabbit cardiac septum (Frank and Langer, 1974). It is of note that the widths of the *ec* and *is*1, which are expressed in absolute values, could be slightly overestimated, taking into consideration swelling of the isolated buffer-perfused heart.

The surface area density of the sarcolemma directly opposing the endothelium and first reached by substances crossing the *is*1 is notably smaller than the surface area density of the remaining part of the sarcolemma lining the non-pericapillary interstitial compartment, *is*2. The former was found to be $89.1x10^3$ m^2/m^3 and the latter, being two times the mid-compartment surface area density of the *is*2, is at least $188x10^3$ m^2/m^3. It is noteworthy that distinction between the respective parts of the sarcolemma facing *is*1 and *is*2 was not made in previous studies dealing with intra-cardiac transfer of lipophilic substances (Bassingthwaighte et al., 1989; Musters et al., 2006).

The fractional volumes of cardiomyocytes and interstitial cells found in the present rabbit study corroborate those observed earlier in rat and rabbit (Frank and Langer, 1974; Anversa et al., 1983, 1985). The fractional volume of interstitial cells found in rabbit myocardial tissue, however, is about 4 times smaller than the value published for dog myocardium (Gerdes and Kasten, 1980).

The present data are useful for studies investigating the uptake, storage and intramyocardial transfer of blood-borne substances. Under normal conditions, cardiac energy conversion heavily depends on the oxidation of fatty acids in the mitochondria of the cardiac muscle cells. The poorly water-soluble fatty acids are supplied to the heart either bound to plasma albumin or attached to a glycerol backbone in circulating triacylglycerols. Before mitochondrial oxidation or storage in the intracellular triacylglycerol pool, fatty acids have to cross the endothelium lining the capillary compartment, the perivascular interstitium, the sarcolemma and the cardiomyocyte cytoplasm. This implies crossing of at least three membrane barriers: the luminal and abluminal endothelial membrane and the sarcolemma. Until now, the mechanisms underlying the uptake, intramyocardial transport and storage of blood-borne fatty acids in the heart are still incompletely understood. Insight can be obtained by studies on intact hearts, among others, by making use of multiple indicator dilution techniques (Bassingthwaighte et al., 2006). To interpret the outcome of these studies properly, detailed quantitative information about cardiac ultrastructural dimensions as presented in our study is required.

In conclusion, in the present study in the adult, glutaraldehyde-perfusion fixed rabbit heart we measured the volume fractions of myocardial compartments such as that of the capillaries, large vessels, endothelium, interstitium (*is*1 and *is*2) and cardiomyocytes, Moreover, we assessed the diffusional width of the endothelial and *is*1 compartments and the surface area of the luminal and abluminal endothelial cell membranes and of the membranes of the cardiomyocytes facing *is*1 or *is*2. These data are required for studies aiming at elucidating the mechanisms underlying the uptake and intramyocardial transfer of hydrophobic substances such as blood-borne fatty acids.

Appendix

Distribution of capillary eccentricity with models OBLIQUE and ELLIPSE

In the *LoMagEm* images, we intended to cut the myofibers perpendicularly. The most likely direction of the capillaries was assumed to coincide with that of the fibers. In the images, the majority of the capillary cross-sections appeared to be ellipsoidal. Generally, the major axis of the ellipsoidal cross-sections had a preferential orientation that we attributed to non-perpendicular sectioning of the slices. To correct for this artefact we compressed the image along that preferential direction, just so that an image with ellipsoidal cross-sections without preferential orientation remained. This image was used for further analysis.

To reliably assess capillary diameter, it is essential to know whether after this compression the ellipsoidal cross-section is merely due to oblique sectioning of the individual cylindrical capillaries around the perpendicular axis (model *OBLIQUE*) or that the capillaries are truly ellipsoidal in nature (model *ELLIPSE*). We analyzed a large number of capillary cross-sections (n=2238) and assessed the statistical distribution of eccentricity E of the ellipse, as defined according to Equation (1), to discriminate between the two options. To facilitate the statistical analysis we considered the distribution of eccentricity to be two-dimensional with perpendicular components E_{xx} and E_{xy}, depending on magnitude of eccentricity E and direction φ of the long axis of the ellipsoidal cross-section. Thus, we used (equation 14):

$$E_{xx} = E\cos(\varphi) \quad E_{xy} = E\sin(\varphi)$$

According to model *ELLIPSE*, the cross-section of a capillary is ellipsoidal in such a way that the parameters E_{xx} and E_{xy} are normally distributed around the origin $[E,\varphi]= [0,0]$, expressed by the two-dimensional probability density functions (equation 15):

$$p_{xy}(E_{xx},E_{xy}) = \frac{1}{\pi\sigma_E^2}\exp\left(\frac{E_{xx}^2+E_{xy}^2}{\sigma_E^2}\right)$$

Parameter σ_E represents dispersion of eccentricity. Since we measured the probability of eccentricity E, a conversion can be made to the polar coordinates $[E,\varphi]$ by substitution of Equation (14) into Equation (15). After integration over the perimeter, defined by the interval $0<\varphi<2\pi$, for the one-dimensional probability density function of eccentricity $p_{E,ellipse}(E)$, it follows that (equation 16):

$$p_{E,ellipse}(E) = \int_0^{2\pi} p_{xy}(E_{xx},E_{xy})Ed\varphi = \frac{2E}{\sigma_E^2}\exp\left(-\frac{E^2}{\sigma_E^2}\right)$$

Because in model *ELLIPSE*, we considered the capillary cross-section to be truly ellipsoidal, the perimeter of the ellipse is somewhat larger than the circumference of a circle with equal cross-sectional area. The perimeter, s (equation 17), of an ellipse can be approximated accurately as a function of the long and short axes d_{max} and d_{min} (http://www.mathsisfun.com/geometry/ellipse-perimeter.html) by:

$$s = \pi\sqrt{\frac{d_{max}^2+d_{min}^2}{2}}$$

Using the definition of eccentricity E as described by Equation (1) and using the definition of the cosine hyperbolic function (cosh), Equation (17) can be

rewritten as (equation 18):

$$s = \pi\sqrt{d_{\max}d_{\min}}\sqrt{\frac{\exp(E)+\exp(-E)}{2}} = \pi d_{cap}\sqrt{\cosh(E)}$$

So, as compared to the perimeter of a circle, the perimeter of an ellipse is found by multiplication with a correction factor, namely the square root of cosh (E). As shown in Fig. 6, a best fit was found for σ_E=0.43. It can be derived that σ_E is equal to the mean value E_{cap} of eccentricity E. Substitution of this value in Equation (18) results in a value of 1.046 for the correction factor, used in Equation (4).

According to model *OBLIQUE*, the tangent t of the angle β between the capillary and the perpendicular to the image plane is normally distributed in two dimensions around the origin $[t_x,t_y]$= [0,0]. After conversion to a single coordinate $t=\sqrt{(t_x^2+t_y^2)}$ and integration over the angular coordinate, similar to the derivation of Equation (16), for the probability $p_t(t)$ of tangent t it holds that (equation 19):

$$p_t(t) = \frac{2t}{\sigma_t^2}\exp\left(-\frac{t^2}{\sigma_t^2}\right)$$

Parameter σ_t represents dispersion of tangent t. Tangent t corresponds to eccentricity E by (equation 20):

$$t = \sqrt{\exp(2E)-1}$$

Thus for the *OBLIQUE* related probability density $p_{E,oblique}$, using the E derivative of Equation (20), it is found that (equation 21):

$$p_{E,oblique}(E) = p_t(t)\frac{\mathrm{d}t}{\mathrm{d}E} = \frac{2}{\sigma_t^2}\exp\left(2E+\frac{1-\exp(2E)}{\sigma_t^2}\right)$$

We derived Equation (21) by means of the computer program Mathematica 10 (http://www.wolfram.com). Fig. 6 shows the probability density function of the eccentricity parameter E as defined by Equation (1) for all best fitting ellipses of 2338 capillary cross-sections. In the same figure, we also show these functions as expected based on the models *ELLIPSE* and *OBLIQUE*. In the model *ELLIPSE*, the eccentricity components E_{xx} and E_{xy} are normally distributed around zero, with standard deviation σ_E=0.43.The fit with the experimentally determined histogram appeared to be excellent. In model *OBLIQUE*, i.e., attributing eccentricity merely to oblique sectioning of the individual capillaries, zero eccentricity would be most probable with probability decreasing continuously with increasing eccentricity. Fig. 6 indicates that this is clearly not the case in the experiments.

Furthermore, calculation of the *OBLIQUE* probability density function as shown in Fig. 6, revealed a standard deviation of the tangent of capillary orientation of 56°. This value is unrealistically high, because it approaches the absence of a relationship between fiber and capillary orientation. In summary, we rejected the *OBLIQUE* model and accepted the *ELLIPSE* model for further analysis of our data. Accordingly, the surface areas of the ellipsoidal capillaries are presented in table 1.

Acknowledgements. Benoit-Giles Kerfant and Stijn Lumeij are acknowledged for their expert help in heart perfusion and Marie-Hélène Lenders for her contribution in tissue fixation and light- and electron-microscopic analysis.

The authors declare no conflict of interest, financially or otherwise.

References

Anversa P., Beghi C., Levicky V., McDonald S.L., Kikkawa Y. and Olivetti G. (1985). Effects of strenuous exercise on the quantitative morphology of left ventricular myocardium in the rat. J. Mol. Cell. Cardiol. 17, 587-595.

Anversa P., Levicky V., Beghi C., McDonald S.L. and Kikkawa Y. (1983). Morphometry of exercise-induced right ventricular hypertrophy in the rat. Circ. Res. 52, 57-64.

Bassingthwaighte J.B., Noodleman L., van der Vusse G. and Glatz J.F. (1989). Modeling of palmitate transport in the heart. Mol. Cell. Biochem. 88, 51-58.

Bassingthwaighte J.B., Raymond G.M., Ploger J.D., Schwartz L.M. and Bukowski T.R. (2006). GENTEX, a general multiscale model for in vivo tissue exchanges and intraorgan metabolism. Philos. Trans. A Math. Phys. Eng. Sci. 364, 1423-1442.

Blaauw E., van Nieuwenhoven F.A., Willemsen P., Delhaas T., Prinzen F.W., Snoeckx L.H., van Bilsen M. and van der Vusse G.J. (2010). Stretch-induced hypertrophy of isolated adult rabbit cardiomyocytes. Am. J. Physiol. 299, H780-787.

Cieslar J., Huang M.T. and Dobson G.P. (1998). Tissue spaces in rat heart, liver, and skeletal muscle in vivo. Am. J. Physiol. 275, R1530-1536.

Eisenberg B.R. and Mobley B.A. (1975). Size changes in single muscle fibers during fixation and embedding. Tissue Cell. 7, 383-387.

Frank J.S. and Langer G.A. (1974). The myocardial interstitium: its structure and its role in ionic exchange. J. Cell Biol. 60, 586-601.

Gerdes A.M. and Kasten F.H. (1980). Morphometric study of endomyocardium and epimyocardium of the left ventricle in adult dogs. Am. J. Anat. 159, 389-394.

Gonzalez F. and Bassingthwaighte J.B. (1990). Heterogeneities in regional volumes of distribution and flows in rabbit heart. Am. J. Physiol. 258, H1012-1024.

Judd R.M. and Levy B.I. (1991). Effects of barium-induced cardiac contraction on large- and small-vessel intramyocardial blood volume. Circ. Res. 68, 217-225.

Macchia D.D., Page E. and Polimeni P.I. (1979). Interstitial anion distribution in striated muscle determined with [35S]sulfate and [3H]sucrose. Am. J. Physiol. 237, C125-130.

Mandarim-de-Lacerda C.A. (2003). Stereological tools in biomedical research. An. Acad. Bras. Cienc. 75, 469-486.

McElroy C.L., Gissen S.A. and Fishbein M.C. (1978). Exercise-induced reduction in myocardial infarct size after coronary artery occlusion in the rat. Circulation 57, 958-962.

Muhlfeld C., Nyengaard J.R. and Mayhew T.M. (2010). A review of

state-of-the-art stereology for better quantitative 3D morphology in cardiac research. Cardiovasc. Pathol. 19, 65-82.

Musters M.W., Bassingthwaighte J.B., van Riel N.A. and van der Vusse G.J. (2006). Computational evidence for protein-mediated fatty acid transport across the sarcolemma. Biochem. J. 393, 669-678.

O'Keefe D.D., Hoffman J.I., Cheitlin R., O'Neill M.J., Allard J.R. and Shapkin E. (1978). Coronary blood flow in experimental canine left ventricular hypertrophy. Circ. Res. 43, 43-51.

Page E. and Page E.G. (1968). Distribution of ions and water between tissue compartments in the perfused left ventricle of the rat heart. Circ. Res. 22, 435-446.

Polimeni P.I. and Buraczewski S.I. (1988). Expansion of extracellular tracer spaces in the isolated heart perfused with crystalloid solutions: expansion of extracellular space, trans-sarcolemmal leakage, or both? J. Mol. Cell. Cardiol. 20, 15-22.

Saburkina I., Gukauskiene L., Rysevaite K., Brack K.E., Pauza A.G., Pauziene N. and Pauza D.H. (2014). Morphological pattern of intrinsic nerve plexus distributed on the rabbit heart and interatrial septum. J. Anat. 224, 583-593.

van der Vusse G.J., van Bilsen M., Glatz J.F., Hasselbaink D.M. and Luiken J.J. (2002). Critical steps in cellular fatty acid uptake and utilization. Mol. Cell. Biochem. 239, 9-15.

Vinnakota K.C. and Bassingthwaighte J.B. (2004). Myocardial density and composition: a basis for calculating intracellular metabolite concentrations. Am. J. Physiol. 286, H1742-1749.

Waits C.M., Barr R.C. and Pollard A.E. (2014). Sensor spacing affects the tissue impedance spectra of rabbit ventricular epicardium. Am. J. Physiol. 306, H1660-1668.

Wang L., Myles R.C., De Jesus N.M., Ohlendorf A.K., Bers D.M. and Ripplinger C.M. (2014). Optical mapping of sarcoplasmic reticulum Ca2+ in the intact heart: ryanodine receptor refractoriness during alternans and fibrillation. Circ. Res. 114, 1410-1421.

Accepted September 7, 2015